Catalysis Today 164 (2011) 451–456

Contents lists available at ScienceDirect

Catalysis Today

journal homepage: www.elsevier.com/locate/cattod

Performance of bifunctional Pd/M_xN_yO (M = Mg, Ca; N = Zr, Al) catalysts for aldolization–hydrogenation of furfural–acetone mixtures

Laura Faba, Eva Díaz, Salvador Ordóñez*

Department of Chemical Engineering and Environmental Technology, University of Oviedo (Faculty of Chemistry), Julián Clavería s/n, 33006 Oviedo, Spain

ARTICLE INFO

Article history:
Received 1 July 2010
Received in revised form 9 November 2010
Accepted 13 November 2010
Available online 9 December 2010

Keywords:
Basic catalysis
Biomass-upgrading
Basic mixed oxides
2nd generation biofuels

ABSTRACT

The performance of different bi-functional Pd catalysts (supported on Mg–Zr, Mg–Al and Ca–Zr mixed oxides) for the aqueous-phase aldol-condensation of acetone and furfural was studied in this work. Experiments were carried out in a batch slurry reactor at 323–393 K. Activity trends, as well as selectivity for the formation of the different adducts (C_8 and C_{13}), were correlated with the physico-chemical properties of the materials, mainly with the distribution of acid and basic sites. In general, it was observed that the catalyst with the lowest concentration of basic sites (Pd/Ca–Zr) presents the poorest performance. By contrast, the presence of medium-strength acid sites (as the observed in the case of one the Pd/Mg–Al catalyst) seems to enhance the catalytic activity of the material. Although selectivities trends were similar for the catalysts supported on Mg–Zr and Mg–Al catalysts, the ability of the materials for catalyzing the formation of the heaviest adducts depends mainly on the total concentration of basic sites.

1. Introduction

Renewable energies are nowadays a major technological challenge because of both the fossil fuels depletion and the environmental concerns about greenhouse gases emissions [1]. Among these renewable energy sources, biomass-based processes are the only able to produce organic fuels at relevant amounts, because of the carbon content of the biomass. The main first generation biofuels are bioethanol, used as a gasoline substitute, and biodiesel, produced from vegetable oils after conversion into the corresponding fatty acid methyl esters. These processes have several drawbacks, such as the competition with food crops, and the low efficiency in terms of fraction of biomass carbon atoms transformed into fuels [2].

In order to overcome these problems, efforts are focused on developing the so-called second generation biofuels, which are expected to be better in terms of energy balances and greenhouse gas emission reduction; as well as for avoiding the problems of competition with food and for water resources. There is still much work to be done to improve the existing processes and for the development of new efficient technologies. The most effective and efficient utilization of renewable biomass resources is through the development of an integrated biorefinery, in which the energy requirements of each process are balanced with those of other processes analogous to petroleum refinery [3]. Among the proposed processes (thermochemical, biological, chemical processes), those consisting of low-temperature hydrolysis of cellulosic materials (both chemically or enzymatically promoted) are the most promising. The final product of these hydrolyses are both single sugars (C_5–C_6) and oxidized/dehydrated derivatives of these sugars (furfural, hydroximethylfurfural, etc.). The transformation of the resulting sugars onto these derivatives involves dehydration reactions which can be easily carried out [4]. Direct hydrogenation of all these compounds will lead to C_6 hydrocarbons of low cost [5], but performing a condensation (because of the carbonyl groups of the dehydrated molecules) of some of these units prior the deep hydrogenation step will lead to C_9–C_{15} hydrocarbons, very valuable as diesel fuels. A pioneer work of Prof. Dumesic group [6] explored this possibility, summarizing the advantages expected from this process (low energy consumption, high carbon atom efficiency, easiness of purification steps, etc.). In subsequent papers, these authors proposed as model reaction for catalyst and process development the system furfural–acetone mixtures (furfural can be obtained by sugar dehydration, whereas acetone can also be obtained from biomass) [7]. In summary, these authors proposed a process consisting of the aldol condensation of both species (acetone can condense with one or two furfural molecules, yielding C_8 or C_{13} species), followed by the deep hydrogenation of formed adducts. However, as the process is carried out in aqueous phase, it can be limited by the low solubility of adducts. Thus, a subsequent hydrogenation under mild conditions has been proposed [8]. During this hydrogenation, carbonyl functional groups are transformed into hydroxyl groups, the resulting adducts increasing the solubility.

* Corresponding author. Tel.: +34 985 103 437; fax: +34 985 103 434.
E-mail address: sordonez@uniovi.es (S. Ordóñez).

0920-5861/$ – see front matter © 2010 Elsevier B.V. All rights reserved.
doi:10.1016/j.cattod.2010.11.032

Therefore, the proposed process requires catalysts with basic properties (required for the aldol condensation) and metal phases (mainly Pd). Among basic materials, basic mixed oxides are the first choice for this kind of applications. Although different oxides have been proposed (Mg–Al, Mg–Zr, Mg–Ti) [9–11], there are not, to the best of our knowledge, systematic studies relating the activity of these catalysts with their basic properties. In other applications of chemical reactions catalyzed by basic materials, such as conversion of 2-propanol in propanone [12], the decomposition of 2-methyl-3-bunil-2-ol [13], transesterification reactions [14], Knoevenagel condensation [15] or aldol condensation [16], it was observed that aspects as the concentration of basic sites and the distribution of the basicity strength of these materials play a key role on the catalytic performance.

The present work tries to fill this gap. For accomplishing this purpose, three different basic solids were used to prepare bi-functional basic-metal catalysts. The first one is a Mg–Zr mixed oxide, the best support among the tested in the published works specifically devoted to study this reaction [7–9]. A hydrotalcite-derived Mg–Al support was also considered, based on a previous work of our research group, in which the preparation procedure (saturation conditions, ultrasonication, etc.) has been optimized in order to obtain enhanced basic properties of the material [17]. The third considered support is a Ca–Zr support, prepared according to the method proposed by Liu et al., which leads to a mesoporous material with enhanced basicity [18,19]. Concerning to the palladium addition, the conventional incipient wetness impregnation was compared to the isoelectric point impregnation method, proposed by Lambert et al. [20] for the preparation of highly dispersed catalysts. Comparison was done both in terms of catalytic performance and on the effect of palladium addition on the physico-chemical properties of the material.

2. Experimental

2.1. Catalysts preparation

Mg–Al layered double hydroxides (LDH) with Mg/Al ratio of 3 were synthesized by co-precipitation at low super-saturation conditions (constant pH), according to the previously optimized procedure [17]. The material was prepared mixing 1 M solutions of $Mg(NO_3)_2{\cdot}6H_2O$ (Fluka, >99%) and $Al(NO_3)_3{\cdot}9H_2O$ (Panreac, 98%) in 3/1 molar ratio. A volume of 150 mL of this solution was added drop wise to 100 mL of K_2CO_3 (Panreac, 99%) 0.2 M under sonication at 298 K. The pH was kept at 10 by adding appropriate quantities of 1.6 M NaOH (Prolabo, 98%) solution. After that, the precipitate was separated by high-speed centrifugation, washed in deionized water in order to remove the alkali metals and the nitrate ions until pH 7, and dried in oven at 373 K for 24 h. The resulting hydrotalcites were calcined in air flow at 723 K for 7 h to obtain the mixed oxides.

Magnesia–zirconia ($MgO–ZrO_2$) catalyst was synthesized using the sol–gel technique described by Aramendía et al. [15]. The catalyst was prepared by dissolving 50.9 g of magnesium nitrate hexahydrate (Fluka, >99.0%) and 4.04 g of ziconyl nitrate (Aldrich, hydrated) in 1 L of deionized water. The mixture was stirred at room temperature, and a NaOH (Prolabo, 98%) water solution was added until the pH was equal to 10. The gel was aged for 72 h, filtered and washed with deionized water until pH 7. It was dried at 393 K during 24 h and, finally, it was calcined in O_2 (100 cm^3/min) at 3.3 K/min until 873 K, and hold at this temperature 3 h.

Mesoporous $CaO–ZrO_2$ nano-oxide was prepared by a solid–gel route, according to the method described by Liu et al. [19]. One gram of amphiphilic poly(alkylene oxide) block copolymers ($PEO_{20}PPO_{70}PEO_{20}$, Pluroni P123) (Aldrich) was dissolved in 40.21 mL of absolute ethanol (Panreac, 99.5%). As the surfactant was completely dissolved, 1.01 g of calcium nitrate (Panreac, 99.0%) was added. To this solution, 4.45 g of zirconium(IV) *n*-propoxide (Aldrich, 70 wt% solution in 1-propanol) mixed with 0.5 g of acetylacetone (acac) (Panreac, 99%) was added with vigorous stirring, herein acetylacetone acted as a stabilizer to prevent the fast hydrolysis of the zirconium(IV) *n*-propoxide. Upon stirring at room temperature for 1 h, 1.8 g of deionized water was added drop wise. The mixture was gelled in a closed vessel at 323 K for 24 h. Then, the products were washed with deionized water and filtered to remove the residual Na^+. Finally, the sample was heated in flowing He at a heating rate of 5 K/min to 973 K.

The $Pd/MgO–Al_2O_3$, $Pd/MgO–ZrO_2$ and $Pd/CaO–ZrO_2$ catalysts (2% Pd) were prepared by incipient wetness impregnation of Pd (using 10 wt% Pd in tetraaminopalladium(II) nitrate solution from Aldrich) onto the mixed oxides. Resulting materials were calcined in flowing O_2 (100 cm^3/min) with a 2 h ramp and a 2 h hold at 723 K and reduced in flowing H_2 (50 mL/min) with a 1 h ramp and 2 h hold at 473 K. In order to improve the metal dispersion, the $Pd/MgO–Al_2O_3$ was also prepared for another method, using the so-called isoelectric point method [20]. The support was soaked in water solutions of various starting pHs in order to know the point of zero charge (PZC) of the solid. This will be the pH (13) of the palladium aqueous solution. The conditions of calcination and reduction were the same as in the previous method. This catalyst was labeled as Pd/Mg–Al (iso).

2.2. Catalysts characterization

The crystallographic structures of the mixed oxides were determined by XRD using a Philips PW 1710 diffractometer, working with the Cu-K_α line (λ = 0.154 nm) in the range 2θ between 5° and 85° at a scanning rate of 2θ of 2°/min. Specific surface areas and pores volume were estimated by nitrogen adsorption at 77 K in a Micromeritics ASAP 2020 surface area and porosity analyzer. With the same instrument, metal dispersion was estimated by hydrogen chemisorption at 373 K.

The strength and distribution of the basic/acid sites were determined by temperature programmed desorption of preadsorbed CO_2/NH_3 in a Micromeritics TPD/TPR 2900. For CO_2-TPD, samples (10 mg) were treated in He at 723 K for 2.5 h and exposed to a CO_2 stream at 323 K temperature until saturation coverage were reached. Weakly adsorbed CO_2 was removed by flushing with He at the same temperature for about 1.30 h. The temperature was then increased at a linear rate of 5 K/min from 293 K to 723 K and the rate of CO_2 evolution was monitored by mass spectrometry. The same method and equipment was used for NH_3-TPD, saturating with NH_3 (5% in helium).

Used catalysts were analyzed by TPO, using the same device, in order to determine the amount of carbon deposits formed during the reaction. After the pretreatment with He at 723 K for 2 h, the samples were exposed to a O_2 stream while the temperature was increased 5 K/min from 293 K to 873 K. The evolutions of CO and CO_2 signals were monitored by mass spectroscopy. Further details about characterization techniques used in this article can be found in previous works [21,22].

2.3. Reaction studies

Reactions were carried out in a 0.5 L stirred batch autoclave reactor (Autoclave Engineers EZE Seal) equipped with a PID temperature controller and a back pressure regulator. The reactor was loaded with 0.25 L of a 1 mol/L aqueous solution of furfural (Panreac, 98%) and the catalyst (2 g, with an average particle diameter of 50–80 μm), and air is purged out by adding nitrogen up to 55 bar for three times before starting the condensation reaction. The reactor was then pressurized to 10 bar with N_2, heated to 323 K, and stirred

Table 1
Main physicochemical properties of the catalysts and supports used in this work: morphology (N_2 physisorption), metal dispersion (H_2 chemisorption), and CO_2- and NH_3-TPD data.

Catalysts	S_{BET} (m^2/g)	D_p (Å)	V_p (cm^3/g)	Metal dispersion[a] (%)	TPD-CO_2		TPD-NH_3	
					Temperature (K)	μmol/m^2	Temperature (K)	Relative concentration[b]
$MgO–ZrO_2$	78	342	0.804	–	427	1.72	353	116
$Pd/MgO–ZrO_2$	101	172	0.51	61.8	443	1.00	487	1.7
$MgO–Al_2O_3$	168	235	1.09	–	353	1.00	370	14
$Pd/MgO–Al_2O_3$	242	55	0.37	7.4	363	0.40	366	12
$Pd/MgO–Al_2O_{3(iso)}$	162	199	0.84	9.2	413	0.81	281	11
$CaO–ZrO_2$	156	57	0.25	–	437	0.23	473	1
$Pd/CaO–ZrO_2$	184	54	0.26	61.9	353	0.23	560	1.5

[a] Measured by hydrogen chemisorption.
[b] Relative surface concentration of acid sis, measured comparing the ammonia release with the corresponding to the Ca–Zr mixed oxide (studied material with lower surface acidity).

at 1000 rpm for 24 h. Then, acetone (Panreac, 99.5%) was introduced to start the reaction (the resulting concentration of acetone being 1 mol/L, corresponding to a furfural/acetone molar ration of 1). Aldol-condensation was stopped after 24 h of reaction time, and the reactor was then cooled to room temperature. The hydrogenation reaction was started by a similar purging procedure with H_2 and pressurizing the reactor to 44 bar before heating. The stirring speed was maintained at 1000 rpm and the reactor was heated to 393 K at which time H_2 was added to reach a pressure of 55 bar.

Samples were withdrawn from the sampling port during the condensation reaction, filtered, extracted in ether (using a volume relation of 1:1) and analyzed by capillary GC in a Shimadzu GC-2010 equipped with a FID detector, using a 15 m long CP-Sil 5 CB capillary column as stationary phase. Peak assignment was performed by GC–mass spectra and responses were determined using standard calibration mixtures. GC analyses of the samples, as well as the calibration standards, were performed after an extraction with diethyl ether.

3. Results and discussion

3.1. Characterization of fresh catalysts

Crystalline structures of the four catalysts studied in this work, as well as the parent mixed oxides, were studied by XRD. If the bulk mixed oxides are considered, similar trends to those reported in the literature were observed. Periclase ($2\theta = 37^\circ, 43^\circ$ and 62°) and cubic MgO ($2\theta = 29^\circ$ and 38°) are the only crystalline phases observed for the hydrotalcite-derived Mg–Al mixed oxides (Al is expected to be either or very disperse or in amorphous phases), whereas in the case of Mg–Zr mixed oxide both periclase and tetragonal ZrO_2 ($2\theta = 30^\circ$ and 49°) were clearly appreciated. In the case of Ca–Zr mixed oxide, a very amorphous material is observed (in good agreement with the used preparation procedure), width peaks corresponding to tetragonal ZrO_2 are the only diffraction peaks observed.

For Mg–Zr and Ca–Zr mixed oxides, palladium addition has not any noticeable effect on the XRD diffraction patterns of the materials, whereas a slight displacement to lower diffraction angles was observed for both preparation procedures in the case of the Mg–Al mixed oxides. The laminar nature of these materials explains this behavior, the interaction of the material layers with water leads to an increase of the interlayer distances [23].

The main morphological parameters (obtained by nitrogen physisorption and using the BET and BJH approaches for estimating surface area and pore volume, respectively) are summarized in Table 1. All the tested materials present a markedly mesoporous character, as expected considering the properties of these materials reported in the literature. In the three cases, the palladium introduction increases the surface area and decreases the pore volume, since the introduction of palladium swells the crystalline structure, clogging of the pores but increasing the specific surface of the materials. The Mg–Zr catalysts have the lowest surface area, whereas Mg–Al ones the highest. Concerning to the metal dispersion (measured by H_2 chemisorption), it is noticeable that Ca–Zr and Mg–Zr mixed oxides lead to the highest metal dispersions, whereas both impregnation procedures used for the Mg–Al materials do not lead to significant variations on the obtained metal dispersions.

The surface concentration of basic sites, as well as their strength distribution, has been determined by CO_2-TPD. The results are also summarized in Table 1, whereas Fig. 1 shows the TPD profiles, indicating the distribution of these sites. $MgO–ZrO_2$ and $Pd/MgO–ZrO_2$ show higher surface concentration of the strongest basic sites than the other catalysts. Concerning to the effect of the Pd addition on the basicity of the materials, it is observed that in the case of Mg–Zr mixed oxide, the total concentration of basic sites slightly decreases, although the fraction of the strongest ones increases. In the case of the Mg–Al, desorption profiles largely change upon Pd addition, disappearing most of the strongest basic sites of the original mixed oxide. Once again, there are no significant differences at this point between both impregnation procedures. In the case of the Ca–Zr material, Pd impregnation leads to higher concentration of basic sites, but decreases the strength of these sites. According to the literature, basic sites in this kind of materials are located on oxygen ions of low coordination number (stronger sites) or adjacent anionic–cationic pairs (weaker sites) [24].

The acid strength and the relative amount of surface acid sites have been studied by NH_3-TPD. The results are summarized in Table 1, whereas Fig. 1 shows the profiles. In all the catalysts, the presence of palladium markedly decreases the amount of acid centers, although the distribution of these sites remains essentially unaltered. The Mg–Zr double oxide presents the highest concentration of acid sites, attributed to the presence of acid–basic pairs [24], although most of these sites disappear upon Pd addition. Mg–Al mixed oxides presents only weak acid sites, which are less sensitive to Pd addition (no differences were observed in terms of the impregnation procedure), although $Pd/MgO–Al_2O_3$ exhibits also medium-strength acid sites (ammonia release at 650 K). In the case of Ca–Zr mixed oxides, the concentration of acid sites is very low and no significant effects of the Pd addition are observed. The acid sites on this materials are supposed to be located on coordinatively unsaturated trivalent (Al^{3+}) or tetravalent (Zr^{4+}) ions, depending the strength of the acid sites on the geometrical configuration of these unsaturations (tetrahedral or octahedral) [24,25].

The modification of the surface chemistry upon Pd addition is tentatively explained considering the formation of surface hydroxides during impregnation with aqueous solutions, followed by the decomposition of these hydroxides in thermal treatment steps.

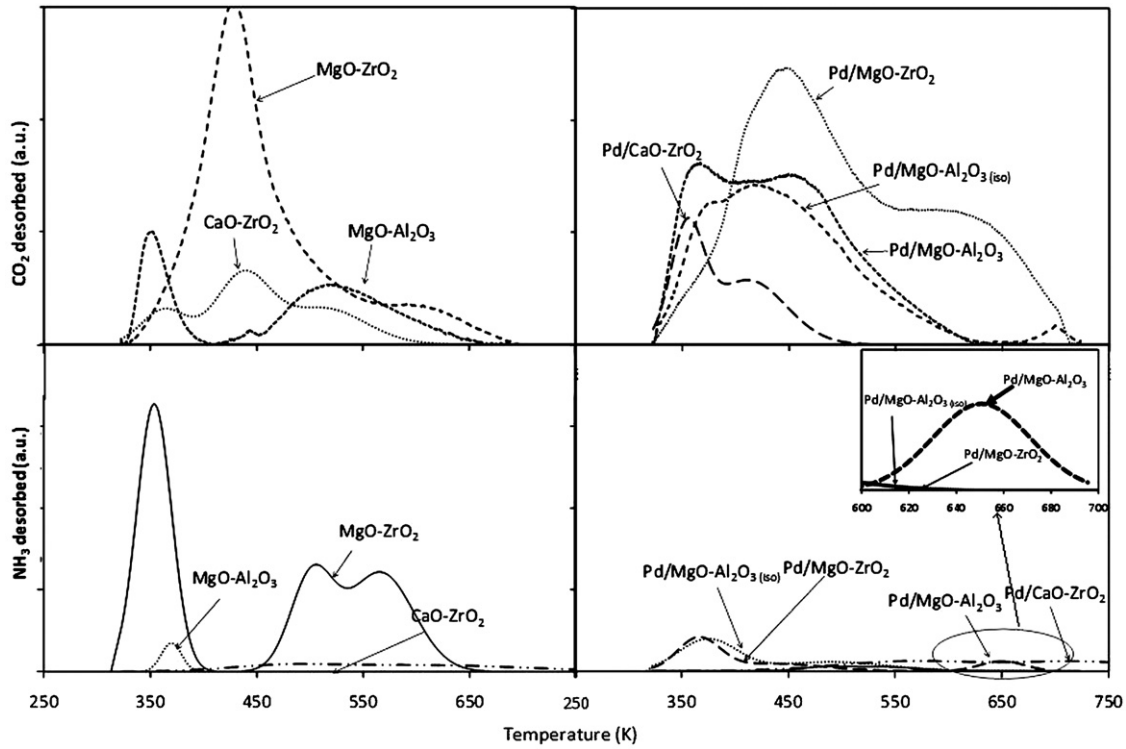

Fig. 1. Patterns of the CO_2 and NH_3 releases obtained for the CO_2- and NH_3-TPDs, respectively, of the considered supports and the resulting bifunctional catalysts.

3.2. Reaction studies

The catalytic activity was evaluated in the aldol condensation of acetone and furfural. The general mechanism, as proposed in the literature for this reaction [7], is depicted in the Scheme 1. It involves the C–C coupling between the carbonyl group of one molecule and the carbonyl α-carbon of the other molecule (in this case acetone, since furfural has no α-H atoms needed for the reaction) to form larger organic molecules. Acetone first reacts with furfural to form C_8 species, which can subsequently react with a second furfural molecule to form a C_{13} molecule. The last adduct will lead to the most valuable hydrocarbon after subsequent deep hydrogenation.

Figs. 2 and 3 show the evolution of the furfural conversion and the selectivities for the different products, respectively. As observed in Fig. 2 (furfural conversion), Pd/MgO–Al_2O_3 shows the best performance in terms of furfural conversion, followed by the Pd/MgO–ZrO_2 catalyst, the Pd/MgO–$Al_2O_{3(iso)}$, and the Pd/CaO–ZrO_2 catalyst. However, the differences among the three first catalysts are negligible once the hydrogenation step is started; remaining the activity of the Pd/CaO–ZrO_2 catalyst markedly lower (the maximum conversion obtained was 50%, whereas all the other catalysts reach total conversion in time interval studied).

Evolution of the selectivity for C_8 and C_{13} adducts with reaction time is shown in Fig. 3. Both selectivities were calculated based on furfural units, as it is shown in the next expression for the case of C_8 selectivity.

$$C_8 \text{ selectivity } (\%) = \frac{\text{mol } C_8}{\text{mol } C_5 + \text{mol } C_8 + 2 \times \text{mol } C_{13}} \times 100 \quad (1)$$

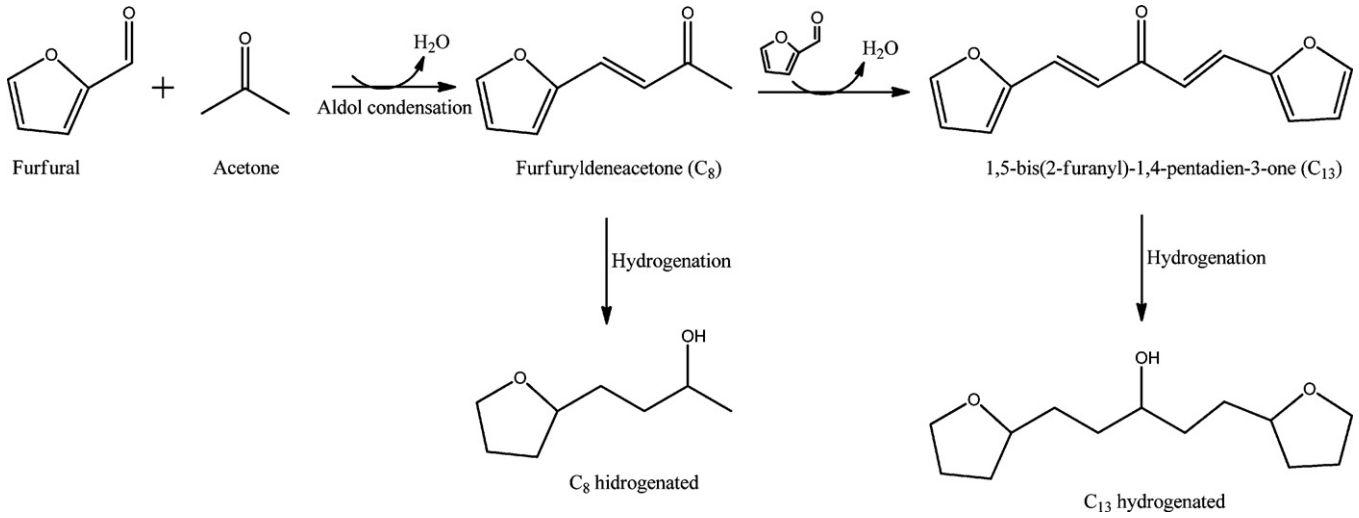

Scheme 1. Reaction network for aldol-condensation and hydrogenation of furfural and acetone.

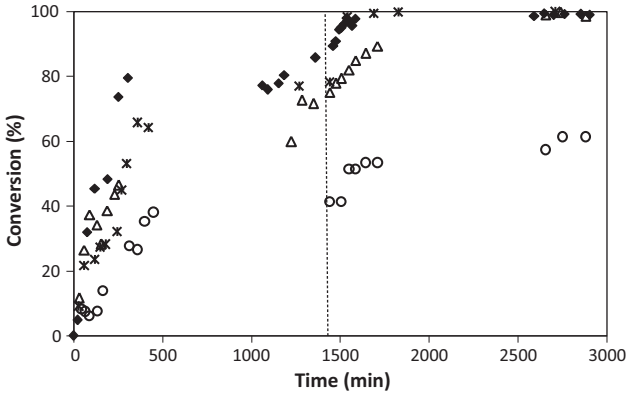

Fig. 2. Evolution of the furfural conversion with the reaction time for aldol-condensation followed by hydrogenation with different catalysts. Pd/MgO–Al_2O_3 (♦); Pd/MgO–$Al_2O_{3(iso)}$ (△); Pd/CaO–ZrO_2 (○); Pd/MgO–ZrO_2 (*). Discontinuous line represents the transition from aldol condensation conditions to hydrogenation conditions.

It is observed that selectivities for the C_8 are systemically higher during the condensation steps, whereas during hydrogenation steps the selectivity to C_{13} systematically increases. This behavior (also observed in the work of Prof. Dumesic group) can be explained considering the low solubility of the C_{13} in the aqueous phase.

Therefore, an important fraction of the C_{13} formed during the condensation phase only can be detected when it is hydrogenated. Consequently, as the selectivity is a relative magnitude, the C_8 selectivity is higher in the condensation.

Overall carbon yield was calculated according to the following expression:

$$\text{Overall carbon yield (\%)} = \frac{3 \times \text{mol } C_3 + 5 \times \text{mol } C_5 + 8 \times \text{mol } C_8 + 13 \times \text{mol } C_{13}}{3 \times \text{mol } C_3 \text{ fed} + 5 \times \text{mol } C_5 \text{ fed}} \times 100 \quad (2)$$

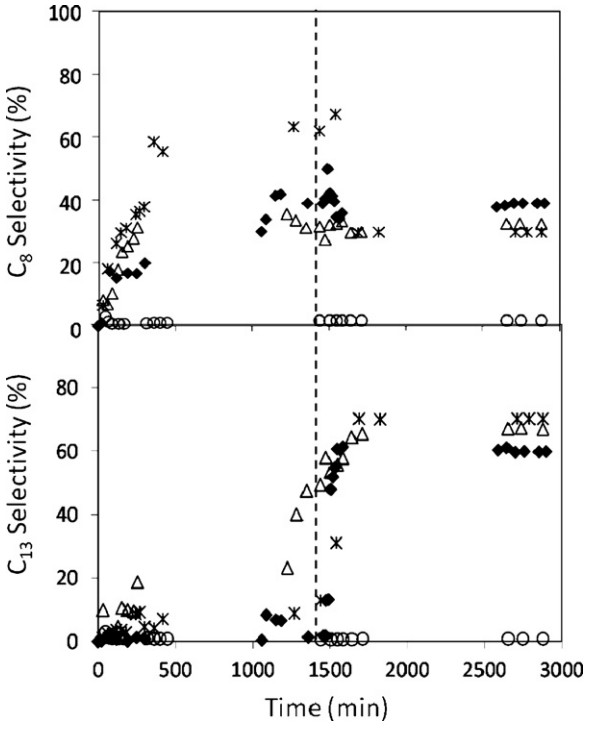

Fig. 3. Evolution of the C_8 and C_{13} selectivity with the reaction time for the different catalysts studied in this work (see Fig. 2 for codes).

It is observed that the closure of the carbon balance decreases markedly at the end of the condensation period, reaching values close to 40% for the catalysts supported on the Mg–Al mixed oxide. That is so because of the limited solubility of these adducts in water (especially in the case of the C_{13} adducts). During the hydrogenation, the solubility of these adducts increases, leading to an increase in the carbon balance closure. In order to corroborate this assumption, separate experiments were performed (with the Pd/MgO–ZrO_2 catalyst) stopping the experiment before the hydrogenation step. Reaction mixture was filtered and the solid was extracted with ether. The same procedure was repeated in the experiment performed with the same catalyst but after the hydrogenation step. The amounts of C_8 compounds were slightly higher (ca. 10%) in the experiment stopped after the condensation step, being this difference markedly higher (ca. 60%) in for the C_{13} fraction composition.

In spite of the increase of the solubility of the condensation adducts upon hydrogenation, Pd/CaO–ZrO_2 and Pd/MgO–$Al_2O_{3(iso)}$ are unable to reach a balance of 100% at the end of hydrogenation phase (balance closure about 90%), whereas the other two catalysts reach the 100% closure. It is related to the formation of other products different of C_8 and C_{13} adducts that do not undergo hydrogenation or are insoluble in aqueous phase in both, condensation and hydrogenation forms. These results are consistent with the worst selectivities for the main products.

In order to identify the extent at which the condensation reactions leading to heavy organic products are taking place, TPO-experiments (not shown) of the used catalysts have been carried out (no CO_2 release peaks were observed during the TPO of fresh catalysts). During these experiments, heavy condensates are oxidized to CO_2 resulting in a signal that can be related to the concentration of these deposits. It was observed that Pd/MgO–Al_2O_3 is the catalyst bearing the greatest amount of carbon deposits. However, Pd/CaO–ZrO_2 presents the lowest amounts of releases CO_2, ruling out the presence of secondary condensation reactions. In addition, combustion temperatures of the carbonaceous deposits of this last catalyst are markedly higher that the corresponding to the other materials, suggesting a different nature of the carbonaceous deposits. Thus, results obtained in the TPO suggest that the formation of the carbonaceous materials is not relevant for justifying neither the reactivity differences nor the lack of carbon balance closure. This fact is reasonable considering the low reaction temperature (390 K) and that the reaction is performed in aqueous phase. Therefore, the non-closure of the carbon balance with the Ca–Zr catalysts is caused by the formation of insoluble intermediates or by the formation of minor amounts of other condensation or degradation products. In good agreement with this observation, the catalysts that are more active for the condensation reaction (as the case of Pd/MgO–Al_2O_3 catalyst) are the catalyst bearing larger amounts of carbonaceous deposits, whereas the Pd/CaO–ZrO_2, which is less active for condensation reaction bears the lowest amounts of carbonaceous deposits.

Taking into account all these considerations, it is concluded that the Pd/CaO–ZrO_2 is not a suitable catalyst for this kind of processes. The main reason for this behavior is the weakness and relatively low concentration of basic sites on this material (Table 1, Fig. 1), significantly lower than the other three materials. Thus, although the acid–basic properties were determined at gas-phase conditions, in general acid/base trends determined in gaseous phase using TPD of probe molecules show good agreement with the reactivity trends for other aqueous phase reactions, as pointed out by West et al. for aqueous-phase butanol dehydration [26].

At the studied reaction conditions, catalysts based on both Mg–Zr and Mg–Al mixed oxides present adequate activities and selectivities for the desired reaction products. If the furfural conversion is taken into account, Pd/MgO–Al_2O_3 presents the highest

activity, followed by Pd/MgO–ZrO_2 and Pd/MgO–$Al_2O_{3(iso)}$. Differences are more marked in the condensation step, when only the basic sites participate in the reaction. This behavior is unexpected at first insight, since both the total concentration of basic sites is lower than the corresponding to the Pd/MgO–ZrO_2, and similar to Pd/MgO–$Al_2O_{3(iso)}$. It suggests that either, the low strength basic sites plays a key role in the activation of the furfural molecule (Pd/MgO–Al_2O_3 has more concentration of the weakest basic sites, as observed in Fig. 1), or that the medium-strength acid sites (as also observed for the Pd/MgO–Al_2O_3 in this figure) can also participate in the furfural activation. At this point, although the mechanism of the aqueous-phase aldol condensation reactions is not so widely studied, gas-phase aldol condensation was considered to be also catalyzed by acid–base pairs [27].

If the selectivities are taken into account, it is observed that the differences among the three materials are very slight. At total conversion, the selectivity to the desired fraction (C_{13}) follows the following order: Pd/MgO–ZrO_2 > Pd/MgO–$Al_2O_{3(iso)}$ > Pd/MgO–Al_2O_3, whereas in the case of the C_8 selectivity, the trend is just the opposite. This result suggests that the higher concentration of basic sites enhances the subsequent condensation.

4. Conclusions

The proposed catalysts are active for the aqueous-phase aldol-condensation of acetone–furfural mixtures. The activity of these materials is closely related to the distribution of both basic and acid sites. Pd/Ca–Zr catalyst presents the worst performance, related to its lower concentration of basic sites, as well as the weakness of these sites.

Pd/MgO–Al_2O_3 catalyst shows the highest furfural conversion, although its basic sites are not the strongest or in a higher concentration. Thus, an influence of the medium-strength basic sites of the material on the catalyst performance can be inferred.

Concerning to the selectivity to the desired fraction (C_{13}), although only slight differences were observed between the Pd/MgO–Al_2O_3 and Pd/MgO–ZrO_2 catalysts, obtained results suggested that the catalysts with higher concentration of basic sites are the most selective for this fraction.

The addition of Pd to the studied basic catalyst largely modifies its acid–base properties. These changes must be taken into account in the rational design of bi-functional condensation–hydrogenation catalysts.

Acknowledgments

This work was supported by the Spanish Government (contract CTQ2008-06839-C03-02). L. Faba thanks the Government of the Principality of Asturias for a Ph.D. fellowship (Severo Ochoa Program).

References

[1] IEA, World Energy Outlook World, International Energy Agency, Paris, 2007.
[2] C. Perego, D. Bianchi, Chem. Eng. J. 161 (2010) 314.
[3] J.N. Chheda, J.A. Dumesic, Catal. Today 123 (2007) 59.
[4] K. Karimi, S. Kheradmandinia, M.J. Taherzadeh, Biomass Bioenergy 30 (2006) 247.
[5] R.M. West, E.L. Kunkes, D.A. Simonetti, J.A. Dumesic, Catal. Today 147 (2009) 115.
[6] G.W. Huber, J.N. Chheda, C.J. Barret, J.A. Dumesic, Science 308 (2005) 1446.
[7] C.J. Barret, J.N. Chheda, G.W. Huber, J.A. Dumesic, Appl. Catal. B 66 (2006) 111.
[8] G.W. Huber, J.A. Dumesic, Catal. Today 111 (2006) 119.
[9] J.I. Di Cosimo, V.K. Diez, C.R. Apesteguia, Appl. Catal. A 137 (1996) 149.
[10] R. Zeng, X. Fu, C. Gong, Y. Sui, X. Ma, X. Yang, J. Mol. Catal. A: Chem. 229 (2005) 1.
[11] B.M. Choudary, M.L. Kantam, P. Sreekanth, T. Bandopadhyay, F. Figueras, A. Tuel, J. Mol. Catal. A 142 (1999) 361.
[12] J.C.A.A. Roelofs, D.J. Lensveld, A.J.v. Dillen, K.P.d. Jong, J. Catal. 203 (2001) 184.
[13] Y. Shigemasa, K. Yokoyama, H. Sashiwa, H. Saimoto, Tetrahedron Lett. 35 (1994) 1263.
[14] A.L. McKenzie, C.T. Fishel, R.J. Davis, J. Catal. 138 (1992) 547.
[15] M.A. Aramendía, V. Borau, C. Jiménez, A. Marinas, J.M. Marinas, J.R. Ruiz, F.J. Urbano, J. Mol. Catal. A: Chem. 218 (2004) 81.
[16] R. Sree, N.S. Babu, P.S.S. Prasad, N. Lingaiah, Fuel Process. Technol. 90 (2009) 152.
[17] M. León, E. Díaz, S. Bennici, A. Vega, S. Ordóñez, A. Auroux, Ind. Eng. Chem. Res. 49 (2010) 3663.
[18] H. Wang, M. Wang, N. Zhao, W. Wei, Y.H. Sun, Catal. Today 115 (2006) 107.
[19] S. Liu, J. Ma, L. Guan, J. Li, W. Wei, Y. Sun, Microporous Mesoporous Mater. 117 (2009) 466.
[20] S. Lambert, N. Job, L. D'Souza, M.F.R. Pereira, R. Pirard, B. Heinrichs, J.L. Figueiredo, J.P. Pirard, J. Regalbuto, J. Catal. 261 (2009) 23.
[21] E. Diaz, S. Ordóñez, A. Vega, J. Coca, Microporous Mesoporous Mater. 82 (2005) 173.
[22] E. Díaz, S. Ordóñez, A. Vega, J. Coca, J. Chromatogr. A 1049 (2004) 161.
[23] D. Carriazo, M. del Arco, C. Martín, V. Rives, Appl. Clay Sci. 37 (2007) 231.
[24] F. Prinetto, G. Ghiotti, R. Durand, D.J. Tichit, Phys. Chem. B 104 (2000) 11117.
[25] H.A. Prescott, Z.-J. Li, E. Kenmitz, A. Trunschke, J. Deutch, H. Lieske, A. Auroux, J. Catal. 234 (2005) 119.
[26] R.M. West, D.J. Braden, J.A. Dumesic, J. Catal. 262 (2009) 134.
[27] J.I. Di Cosimo, V.K. Díez, M. Xu, E. Iglesia, C.R. Apesteguía, J. Catal. 178 (1998) 499.